Gate Manipulation of DNA Capture into Nanopores

Yuhui He,[†] Makusu Tsutsui,[†] Chun Fan,[‡] Masateru Taniguchi,[†,*] and Tomoji Kawai[†,*]

[†]The Institute of Scientific and Industrial Research, Osaka University, 8-1 Mihogaoka, Ibaraki, Osaka 567-0047, Japan and [‡]Computer Center of Peking University, Beijing 100871, China

ABSTRACT Understanding biophysics governing DNA capture into a nanopore and establishing a manipulation system for the capture process are essential for nanopore-based genome sequencing. In this work, the functionality of extended electric field and electroosmotic flow (EOF) during the capture stage and their dependence on gate voltage, U_G, are investigated. We demonstrate that while both the electric field and EOF within a *cis* chamber make long-distance contributions to DNA capture around the pore mouth, the former effect is always capturing, while the latter causes trapping or blocking of the molecule depending on the magnitude of the gate voltage, U_G: an anionic EOF induced by high U_G is capable of doubling the DNA trapping speed and thus the absorption radius in the *cis* chamber, whereas a cationic EOF by low U_G would substantially offset the trapping effort by the electric field and even totally block DNA entrance into the pore. Based on the analysis, a gate regulation is proposed with the objective of achieving a high DNA capture rate while maintaining a low error rate.

KEYWORDS: nanopore sequencing · DNA capture · gate manipulation

The field of electrically detecting and manipulating single molecules passing through a nanopore has witnessed tremendous progress over the past decade.[1,2] Among various applications, nanopore-based genome sequencing has been under intensive studies.[3−5] The idea is to electrophoretically drive negatively charged polynucleotides into a nanopore and identify each constituent nucleotide by monitoring longitudinal ionic current blockage[6−8] or transverse tunneling currents[9−11] while the DNA molecule resides within the pore.

An efficient way of manipulating DNA capture and subsequent nanopore translocation progress is an essential ingredient for the electrical nanopore sequencing. In this aspect, relatively low capture rate was observed in the pioneering SiO_2 nanopore experiments.[12] This was attributed to the wall-surface-charge-induced positive electroosmotic flow (EOF) that moves opposite that of the polynucleotides and thus reduces permeation efficiency[13] (Figure 1a). From then on, several approaches have been developed for the purpose of facilitating DNA capture and translocation. A straightforward method is to increase the longitudinal driving voltage U. Indeed, more frequent capture events are achieved by using larger U.[14,15] However, an accompanying effect is that the molecule speed passing through a nanopore would also get substantially increased due to the larger driving field.[15] This poses a severe obstacle to the sequencing efforts: the two major approaches, one by measuring ionic current blockages and the other by measuring transverse tunnel currents or capacitance, both call for each nucleotide on the penetrating DNA to dwell in the electrical "read" region for more than 1 ms, *i.e.*, with a speed of $\leq$1 base/ms.[4] Another strategy for raising DNA capture rate is to coat the nanopore deliberately with alumina (Al_2O_3) to neutralize the surface charges or even to achieve positive wall surface charges.[13,15] Consequently, the induced negative EOF is now flowing in the same orientation as DNA translocation, enhancing the DNA absorption motion (Figure 1b). Nonetheless, the side effect is very strong pore−polymer affinity since the anionic DNA becomes electrostatically bound to the positively charged wall surface. An effective way to control DNA translocation under such strong interaction for electrical sequencing purposes remains to be seen.

These circumstances present a dilemma on how to facilitate the DNA absorption at the pore entrance while attenuating and regulating the translocation speed inside the pore. From the viewpoint of pore material, Al_2O_3 is beneficial for molecule capture, while it is not appropriate for controlling DNA motion inside a nanopore; on the contrary, SiO_2 is capable of lowering polynucleotide speed permeating the nanopore while reducing the capture rate. As demonstrated in this work, a gate voltage, U_G, has the potential to integrate advantages of both the Al_2O_3 pore and SiO_2 pore by tuning the extended electrical field $E(R)$

* Address correspondence to taniguti@sanken.osaka-u.ac.jp.

Received for review August 19, 2011 and accepted September 19, 2011.

Published online September 19, 2011
10.1021/nn203186c

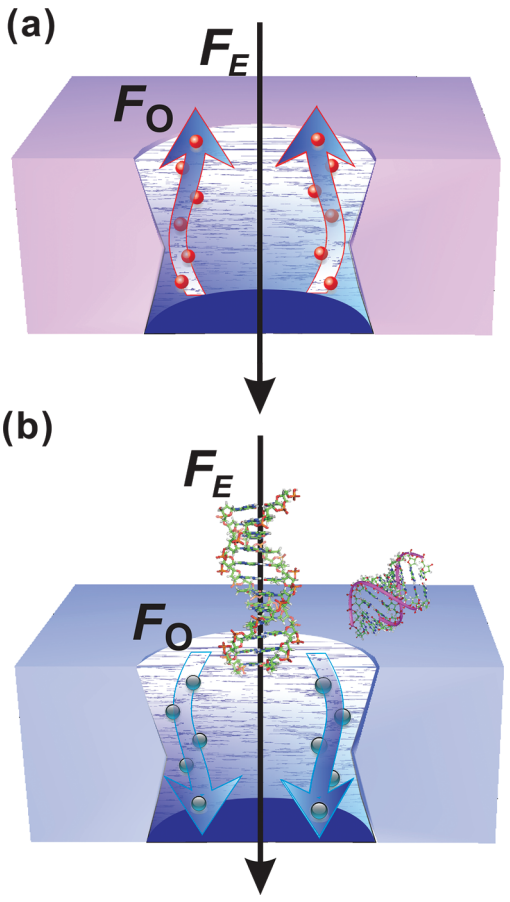

Figure 1. (a) Schematic view of a SiO_2 nanopore with positively charged electrical double layers (EDL), which flows opposite that of negatively charged DNA under electric driving field. In the figure red balls represent net charges of K^+ ions. (b) Similar view of a Al_2O_3 nanopore where EDL are negatively charged and thus flow along the same orientation as that of anionic polynucleotides. The blue balls denote net charges of Cl^- ions. EDL in (a) apply a repulsive force on DNA, leading to reduced capture rates, while those in (b) exert additional forward force on the polymer so that the capture rate is enhanced.

and EOF for DNA motion: a U_G higher than half the driving voltage U would enhance $E(R)$ and induce anionic EOF within the pore, leading to an increased DNA capture rate, as in native Al_2O_3 pores, while a U_G lower than $U/2$ would make the performance like the SiO_2 pore, where the biopolymer penetration is slowed by the cationic EOF. Thus, we propose a gate-control device architecture for DNA capture and translocation: during the capture stage a high gate voltage, U_G, is employed in order to enhance absorption, while a sufficiently low U_G is applied after a polymer gets captured so that other molecules are blocked to avoid sequencing errors.

RESULTS AND DISCUSSION

Capture Kinetics. The DNA capture mechanism around the nanopore entrance is an intriguing phenomenon that involves many physical processes. At present, there is a controversy as to whether the extended electric field from the pore mouth, $E(R)$, or the hydrodynamic convection caused by EOF around the pore entrance, $V(R)$, is the primary factor for driving DNA into the nanopore, as seen in Figure 1b. One theory took account of the continuity of $E(R)$ around the pore mouth and suggested that $E(R)$ can be written as Q/R^2, where Q is the equivalent charge amount at the pore entrance and R is the distance from the entrance.[16−18] However, this argument was criticized as failing to consider the severe screening by counterions within the solution: the Debye length is about 0.3 nm when the salt concentration, N_{KCl}, is 1 M; that is, $E(R)$ would get damped in a few nanometers.[19] As an alternative, it was speculated that the space extension of EOF induced by the nanopore wall surface charges should dominate the DNA-trapping process.[19,20] On the basis of this assumption, an absorption radius model was set up and the calculation results showed nice agreements with experiments using an Al_2O_3 nanopore.[19] Unfortunately, this theory could not explain DNA capture and translocation experiments using a SiO_2 nanopore. As seen in Figure 1a, there could be no absorption region near the nanopore mouth according to the EOF-dominated picture, since EOF induced by SiO_2 wall surface charges flows opposite the electrophoretic DNA motion, whereas successful polynucleotide translocation has been observed in the experiments.[21−24] In our work, we took both electrostatic and hydrodynamic effects into account to explore DNA capture and translocation in a solid-state nanopore.

Figure 1 shows schematic views of DNA capture into SiO_2 (a) and Al_2O_3 (b) nanopores. Here the most significant differences between the two types of pores are the charge signs and directions of EOF. It is known that the surface charges are negative on SiO_2 pore walls,[24,25] whereas they are positive on Al_2O_3 ones.[15,26] Therefore, wall-surface-charge-induced electrical double layers are composed of cations (K^+) for SiO_2 and anions (Cl^-) for Al_2O_3. Under a driving voltage across the nanopore, EOF within SiO_2 pores is in the orientation opposite that of anionic DNA molecules, thus retarding the polymer translocation, and *vice versa* for Al_2O_3 pores. As shown in the figure, impacts of electric field and EOF on the polymer capture can be represented as counteracting $F_E - F_O$ in SiO_2 pores and as reinforcing $F_E + F_O$ in Al_2O_3 pores.

We set up a multiphysics model including electrostatics, hydrodynamics, and ion transport (see Methods section) to implement a quantitative evaluation of electric field, $\vec{E}$, and EOF velocity, $\vec{V}$, in the whole system, as sketched in Figure 2a. R_a is the absorption radius within the *cis* chamber from the pore entrance, defined as the distance translocated by DNA molecules before entering the pore within the Zimm relaxation time:[19,20]

$$\tau_Z = \int_0^{Ra} \frac{dR}{V_{DNA}(R)} \quad (1)$$

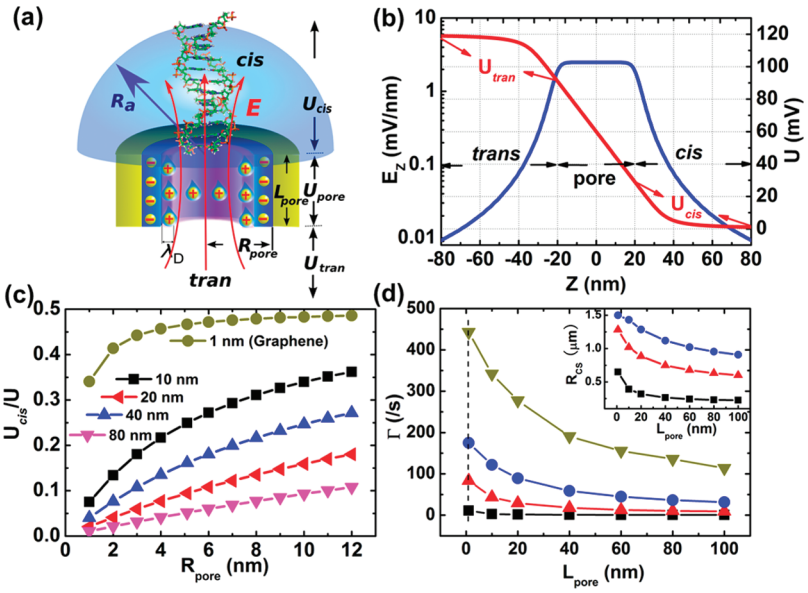

Figure 2. (a) Schematic view of DNA capture into and translocation through an Al_2O_3 cylinder nanopore. The voltage drop is divided into three parts: U_{cis} within the *cis* chamber, U_{pore} within the pore, and U_{trans} within the *trans* chamber: $U = U_{cis} + U_{pore} + U_{trans}$. We can see a sufficiently large voltage residual ratio $\alpha = U_{cis}/U$ is beneficial since large U_{cis} results in a promoted capture rate, while small U_{pore} lowers the polymer translocation speed, thus favoring the electrical interrogation within the nanopore. (b) *Z*-Component electric driving field, E_z, and potential, U, distribution along nanopore *z*-axis. The nanopore length, L_{pore}, is 40 nm, radius R_{pore} is 5.1 nm, salt concentration N_{KCl} = 150 mM, and the applied voltage is U = 120 mV. It demonstrates that E_z decays as $1/R^2$ from the nanopore entrance within the *cis* chamber, rather than exponentially as $\exp(-R/\lambda_D)$, where λ_D is the Debye length, ~0.8 nm. (c) Voltage residue ratio $\alpha = U_{cis}/U$ as a function of nanopore radius, R_{pore}, under various pore lengths, L_{pore}. We note that the situation of the graphene nanopore is explored here as L_{pore} = 1 nm. (d) Capture rate, Γ, as a function of nanopore length, L_{pore}, under various pore radii, R_{pore}. The dark yellow, blue, red, and black lines correspond to R_{pore} = 20, 10, 5.1, and 1 nm, respectively. Here we assume a 60 nM λ-DNA solution is used. Inset plots the critical radius, R_{cs}, for the coil−stretch transition within the *cis* chamber from the pore mouth.

where τ_Z is Zimm relaxation time of the DNA molecule, and V_{DNA} is the local DNA velocity within the *cis* chamber. Near the pore mouth, V_{DNA} is approximated as the sum of drift velocity, V_{dr}, diffusion velocity, V_{di}, and convection velocity, V_c:

$$V_{DNA} = V_{dr} + V_{di} + V_c \approx -\mu_{DNA}E - \frac{D_{DNA}}{R_a} + V \quad (2)$$

where μ_{DNA} and D_{DNA} are electrophoretic mobility and diffusion coefficient of the DNA molecule, and V is the velocity hydrodynamic flow.

We first deduced a potential profile along a nanopore as seen in Figure 2a. The whole driving voltage, U, is made up by three parts: $U = U_{cis} + U_{pore} + U_{tran}$, where U_{pore} is within nanopore, U_{cis} is at the *cis* chamber, and U_{trans} is decreasing at the *trans* chamber. This equation demonstrates the dilemma of previous approaches: in order to increase the polymer capture rate, a larger U is implemented so that U_{cis} is enhanced; however U_{pore} also increases, leading to unwanted high-speed penetration through the nanopore. Hence, in order to achieve a high absorption rate (U_{cis} ↑) and low translocation speed (U_{pore} ↓), the voltage residue ratio $\alpha = U_{cis}/U \approx [2 + (U_{pore}/U_{cis})]^{-1}$ should be maximized in the device design.

Distributions of *z*-component electric field E_z and potential U along the pore axis are plotted in Figure 2b with parameters as in the experiments:[21] R_{pore} = 5.1 nm, L_{pore} = 40 nm, N_{KCl} = 150 mM, and U = 120 mV. This figure demonstrates that the voltage decreases linearly within the pore, while it extends several tens of nanometers into the *cis* and *trans* chambers. The former is ascribed to the small aspect ratio R_{pore}/L_{pore}, and the latter indicates that the screening effect by the counterions is not so strong. This is further illustrated by the distribution of E_z within the *cis* chamber: E_z does not decay exponentially as $\exp(-R/\lambda_D)$, where λ_D is the Debye length, <1 nm; rather, it decays as $1/R^2$ from the pore entrance once $R > 2R_{pore}$. Therefore, our multiphysics modeling identifies that the extended electric field in the *cis* chamber would play a prominent role in DNA capture. The physical mechanism is that the Debye length approximation, originated from the Poisson−Boltzmann equation[19,27] for equilibrium or near-equilibrium transport, becomes invalid for far-from-equilibrium cases such as voltage-driven ion transport here. Our further evaluation indicates that $E(R) \approx E_0(R_{pore}^2/R^2) = U(R_{pore}^2/2L_{pore}R^2)$ suggested by previous work[16−18] is a good approximation for nanopores with small aspect ratio R_{pore}/L_{pore} and low salt concentration N_{KCl}.

Figure 2c plots the voltage residue ratio $\alpha = U_{cis}/U$ as a function of nanopore radius, R_{pore}, under various pore lengths, L_{pore}. This figure reveals that α would be enhanced with increasing R_{pore}, implying higher yield of polymer capture when using larger radius nanopores.

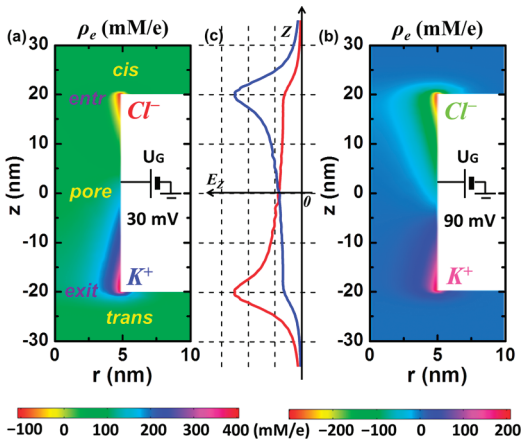

Figure 3. Two-dimensional charge density, ρ_e, in the $z-r$ plane, where gate voltage U_G = 30 mV (a) and 90 mV (b). In the former case, more K^+ ions are accumulated in the channel due to much stronger electric field from the *trans* chamber pointing to the pore; while in the latter case, more Cl^- ions are accumulated. The *z*-component electric field, E_z, along the nanopore *z*-axis is plotted in (c), where the red line is for U_G = 30 mV, and the blue line is for U_G = 90 mV. Parameters are as follows: nanopore radius R_{pore} = 5.1 nm, length L_{pore} = 40 nm, salt concentration N_{KCl} = 150 mM, and driving voltage U = 120 mV, as in typical nanopore experiments.[21] We note that gate dielectrics has been neglected here for convenience; that is, U_G discussed in this work refers to surface potential induced by gate bias in the real experiments.

This is accredited to the weaker screening effect by ions in EOF since the EDL become relatively thinner and farther from the nanopore *z*-axis in larger radius pores (a detailed illustration is provided in the Supporting Information, where the electric field and screening charge distribution along the nanopore *z*-axis are plotted). In addition, for nanopores with the same radii the thicker the nanopore (L_{pore} ↑), the smaller α becomes. It is just as expected, since thicker nanopores would lead to larger potential drops inside the pore, thus reducing residue voltage in the outer chambers. Thus we conclude that a large pore aspect ratio, R_{pore}/L_{pore}, would benefit DNA capture substantially, and this agrees with the experimental observations. Finally, it is worth mentioning that the curve with L_{pore} = 1 nm is plotted with the purpose of investigating capture capability of graphene nanopores. The single- or few-layer graphene nanopores, as ultrathin electrical probes, are believed to achieve single-nucleotide resolution readily,[28] thus becoming one focus of current research.[29−33] From our calculation it seems that given the same pore aspect ratio and driving voltage, graphene nanopores have the largest voltage residue ratio and thus the greatest polymer capture rate. Nonetheless, we note that, on the other hand, the electric field within the pore, $E_{pore} \approx (U - 2U_{cis})/L_{pore}$, is quite large due to graphene thickness, leading to undesirable high translocation speed. As demonstrated in the following section, we will propose gate regulation as a potential solution.

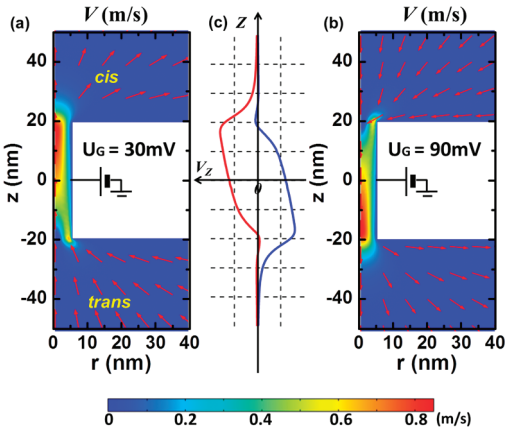

Figure 4. Two-dimensional distribution of liquid velocity, *V*, in the $z-r$ plane, where gate voltage U_G = 30 mV (a) and 90 mV (b). The arrows characterize normalized velocity direction, while the color denotes velocity magnitude. We note that (a) and (b) are equivalent to SiO_2 and Al_2O_3 nanopores, respectively. The *z*-component of the velocity, V_z, along the nanopore *z*-axis is plotted in (c), where the red line is for U_G = 30 mV and the blue line is for U_G = 90 mV. Parameters are set the same as in Figure 3.

We further calculate the capture rate, Γ, defined as those DNA polymers arriving at the nanopore mouth and then successfully overcoming the entropy barrier at the pore mouth:[18,20,34]

$$\Gamma = \Gamma_0 e^{q^*(\Delta U - F_l^\dagger)/k_B T} \quad (3)$$

$$\Gamma_0 = 2\pi R_a^2 c_0 V_{DNA} \quad (4)$$

where Γ_0 characterizes the rate of DNA molecules reaching the pore entrance, ΔU is the electrical capture potential in the *cis* chamber, $F_l^\dagger$ is the entropy barrier height, q^* is the effective charge amount of the DNA chain end, k_B is the Boltzmann constant, T is the temperature of the solution, and c_0 is the far field concentration of DNA molecules. Calculated capture rates based on the above model show good accordance with experimental observations[15] (see Figure S3 and the associated discussion in the Supporting Information). The dependence of Γ on nanopore length, L_{pore}, and pore radius, R_{pore}, is depicted in Figure 2d. The inset plots the associated variance of R_{cs} with L_{pore} and R_{pore}. Here R_{cs} is defined as the critical radius from the nanopore entrance where a DNA coil−stretch transition would happen due to the velocity gradient,[35,19] another quantity evaluating nanopore absorption capability. According to our calculation, R_{cs} is close to R_a quantitatively. By comparing Figure 2d and its inset, we find that the variation tendency of Γ with pore dimension is similar to that of R_{cs}. Therefore, R_a (or R_{cs}) deserves emphasis in the discussion since it determines the experimental observable Γ.

Gate Manipulation. Having analyzed the DNA capture process and its variance with pore material and dimension, we now explore its dependence on gate controlling.

Recently, the successful fabrication of gate-all-around nanopores and nanochannels provides an efficient way of manipulating the ionic transport by gate voltages.[36,37] Since gate voltage is capable of tuning ion charge density in the nanopore, we become aware that this would also be able to manipulate DNA capture at the pore mouth by controlling EOF strength and electric driving field distribution. Here we propose a strategy of regulating DNA capture through gate voltage and give a quantitative study in the following.

Figure 3 plots the net charge distribution in the *cis* chamber, nanopore, and *trans* chamber under driving voltage $U = 120$ mV, with a low gate voltage, $U_G = 30$ mV, and a high one, $U_G = 90$ mV. For both cases, K^+ ions accumulate at the exit of the nanopore, while Cl^- ions accumulate at the entrance, ascribed to the electric driving field pointing from the *trans* chamber to the pore and from the pore to the *cis* chamber. On the other hand, a low gate voltage results in a stronger electric field near the exit of the nanopore, as depicted in Figure 3c, and many more K^+ piling there, while a high U_G achieves the opposite. Now we arrive at one central finding of this work: a gate voltage $U_G < U/2$ induces cationic EDL in the fluid channel, while $U_G > U/2$ does the opposite. The former EDL would flow from the *trans* to the *cis* chamber under driving voltages, thus blocking DNA absorption into the nanopore, while the latter moves in the same direction as DNA trapping, promoting the capture process. This is clearly demonstrated in Figure 4, where two-dimensional hydrodynamic velocity fields, V, in the nanopore radius−axis plane are plotted for $U_G = 30$ and 90 mV. Figure 4c further plots the z-component fluid velocity, V_z, along the nanopore z-axis under $U_G = 30$ mV (red line) and 90 mV (blue line). We stress that from the viewpoint of EOF sign and direction, smaller U_G behaves like those negative surface charges on SiO_2 nanopore walls, while larger U_G makes nanopores perform like Al_2O_3. Finally, it is intriguing to find that V_z becomes largest near the pore entrance when $U_G = 30$ mV, revealing that the blocking effect would be strongest at the pore mouth rather than at the exit. It is a favorable effect for the objective of preventing other polymers from entering the pore when there has already been one inside the nanopore. Here the underlying physics is the continuity principle of liquid flow, as seen in Figure 4a.

In general, Figure 3 depicts the redistribution of electric driving fields in the presence of gate voltage, U_G, while Figure 4 exhibits that of EOF caused by U_G. For the purpose of blocking DNA molecules from absorbing into nanopores, a small gate voltage ($<U/2$) functions in two aspects: on one hand, the electric driving field at the pore entrance gets attenuated due to reduced bias voltage between the pore wall and the *cis* chamber (compare red line and blue line in Figure 3c); on the other hand, more cations are induced in the fluid channel so that EOF rather than DNA capture motion is enhanced, and consequently the liquid outflow from the pore entrance gets reinforced, putting a stronger repelling force on DNA molecules trying to enter the pore (Figure 3a and Figure 4a). For the target of improving DNA capture rate, a large gate voltage contributes also in two aspects: the electric field for absorption at the pore mouth is increased, while the anionic EOF is reinforced, promoting convection velocity of the DNA trapping motion. In brief, a low gate voltage leads to weakened electric capture force and

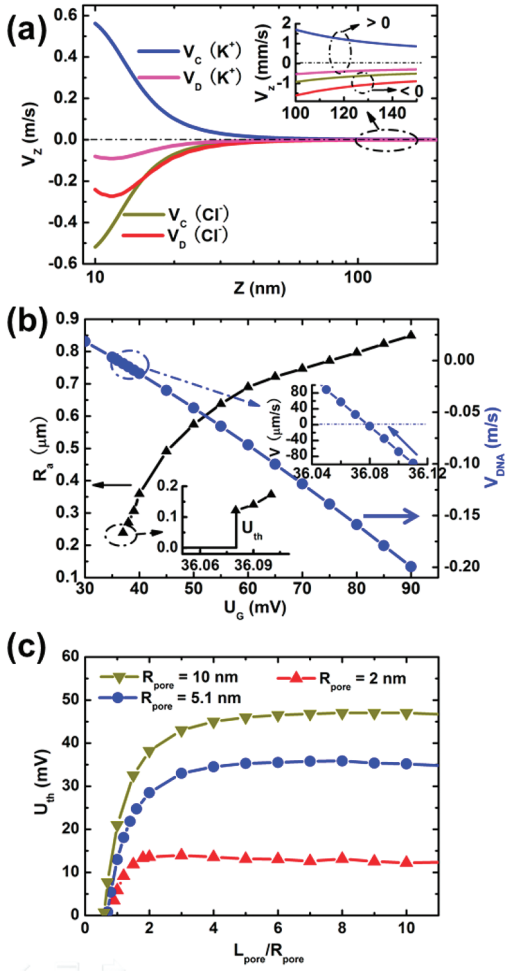

Figure 5. (a) DNA velocity, V_{DNA}, along the z-axis within the *cis* chamber is made up of two components: the drift-diffusion velocity, V_D, mainly determined by extended electric field $E(R)$ from the pore entrance, and the convection velocity, V_c, due to EOF. Here K^+ represents $U_G = 30$ mV where EOF is opposite of DNA capture and translocation (see Figure 4a), while Cl^- characterizes $U_G = 90$ mV (see Figure 4b). The inset gives a detailed view of these velocity components a bit further away from the nanopore: $V_{DNA} = V_C + V_D$ is positive at $U_G = 30$ mV, while it becomes negative at $U_G = 90$ mV. Other parameters are the same as in Figure 3. (b) Absorption radius, R_a, and V_{DNA} at the pore entrance as functions of gate voltage, U_G. Insets give detailed views showing that there exists a threshold voltage $U_{th} \approx 36$ mV, below which DNA could not get into the pore and R_a is zero. (c) Threshold gate voltage, U_{th}, for DNA capture as a function of nanopore aspect ratio, L_{pore}/R_{pore}, under various pore radii, R_{pore}.

strengthened hydrodynamic repulsive force, while a high gate voltage does the opposite.

So far, the dependence of an extended electric field and EOF on gate voltage and their influence on polymer capture have been analyzed qualitatively. Next, we performed a quantitative study of DNA motion under gate voltage. The drift-diffusion velocity, $V_D = V_{dr} + V_{di}$, and convection velocity, V_C, of polynucleotides along the *z*-axis in the *cis* chamber are plotted in Figure 5a (in fact, the diffusion velocity is negligible compared to the drift velocity for λ-DNA capture discussed in this work; a detailed analysis is provided in the Supporting Information). K^+ represents U_G = 30 mV, while Cl^- represents U_G = 90 mV. The pore entrance is located at Z = 10 nm, and the exit at Z = −10 nm. Therefore, DNA molecules with $V_D + V_C < 0$ are capable of being absorbed, while those with $V_D + V_C > 0$ would be driven away from the pore entrance. The inset gives a detailed view of these velocity components at about 100 nm away from the pore mouth. For U_G = 90 mV we find $V_D \approx V_C < 0$. This indicates that a high enough gate voltage would double the DNA trapping speed by inducing negatively charged EOF, and consequently, the absorption radius doubles under high U_G. For U_G = 30 mV, $V_D + V_C > 0$ is observed, indicating the DNA molecule would be expelled away from the pore entrance by the strong hydrodynamic outflow. The threshold voltage below which total blockage of DNA molecules would occur is explored in Figure 5b, where DNA velocity at the pore entrance, V_{DNA}(entr), and absorption radius, R_a, are plotted as functions of gate voltage, U_G. V_{DNA}(entr) keeps increasing as U_G gets lower and finally turns *positive* (inset). Respectively, R_a becomes zero, signifying no capture event could occur now. We would like to mention that below the threshold gate voltage, U_{th}, the positive V_{DNA} should be understood as that some DNA polymer may get close enough to the pore mouth through Brownian motion and then be driven away by the nanopore outflow there.

The dependence of threshold gate voltage, U_{th}, on pore geometry is further investigated in Figure 5c. We find that for nanopores with large pore aspect ratio ($R_{pore}/L_{pore} \rightarrow \infty$) U_{th} does not exist; that is, the DNA molecule could always penetrate the pore regardless of the gate voltage applied. This can be attributed to the weakened gate control ability: the thickness of the gate-manipulated EOF is measured in units of Debye length; thus a sufficiently large pore radius makes its influence weaker and even trivial (though invalid along the transport *z*-axis, Debye length estimation remains a good approximation of nanopore radius direction, as seen in Figure 3a and b). In addition, U_{th} becomes saturated as the pore length increases ($L_{pore}/R_{pore} \uparrow$). Such a saturation behavior originates from the variance of voltage residue ratio, U_{cis}/U, with pore thickness, L_{pore}, as plotted in Figure 2: U_{cis}/U keeps decreasing with increasing L_{pore} and finally stays at the minimum; thereupon the gate voltage required to offset the absorbing effect by U_{cis} also becomes saturated.

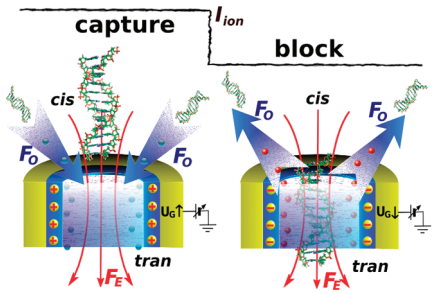

Figure 6. Schematic illustration of gate manipulation of DNA capture *via* feedback of ionic current signal. Blue balls denote Cl^- ions, while red balls represent K^+ ions. The big arrows indicate direction of hydrodynamic flow. Forces exerted on DNA by the driving field and by EOF are characterized as F_E and F_O, respectively. At the capture stage, a larger gate voltage, U_G, is applied for the objective of promoting DNA absorption radius and inducing polymer coil−stretch transition; at the translocation stage, U_G becomes smaller than the threshold for DNA capture, thus preventing other polymers from entering the pore. Switching between the two stages is triggered by the blocking and restoring of ionic current.

From the above results, we propose gate control on the DNA capture process, as seen in Figure 6: at the beginning a high gate voltage, U_G, is exerted with the objective of inducing anionic EOF so that the DNA capture rate is enhanced (capture stage); after successful capturing of a polynucleotide into the nanopore, the variation of longitudinal ionic current triggers a switch of U_G to that below the threshold, leading to the blockage of other polynucleotides into the nanopore, while there has been one translocation inside (block stage); finally, the successful translocation of the current DNA molecule through the pore causes termination of ionic current blockage, which serves as a feedback signal to gate control. It is worth mentioning that at the block stage, the low gate voltage would also substantially lower the translocation speed of the target DNA molecule threading the nanopore.[38] Thus the sequencing requirement of each nucleotide dwelling in the pore for at least 0.1 ms could also get addressed.

CONCLUSION

In summary, we have assessed the influence of electric field and hydrodynamic flow on the DNA capture process and their dependence on gate controlling. Our study demonstrated that a gate bias smaller than half the longitudinal driving voltage would reduce the electric capture field and meanwhile promote the cationic electroosmotic flow, which blocks DNA from entering the pore, thus suppressing the DNA capture process. Quantitatively a threshold gate voltage is identified below which no polymer absorption could occur. On the other hand, a higher

gate voltage would perform oppositely, enhancing the absorption radius substantially. On the basis of the analysis, we have proposed a feedback gate manipulation of the DNA capture process, with the potential of promoting the capture rate and minimizing the sequencing error rate. Our results can provide guidelines for the experimental gate manipulation of DNA capture and translocation through solid-state nanopores.

METHODS

A two-dimensional *z*-axis symmetric model calculating ion transport, laminar flow, and electrostatics along the *z*-direction and nanopore radial direction was built with COMSOL (School of Mathematical Sciences, Peking University):

(1) Poisson equation for electrostatics:

$$\nabla \cdot \vec{E} = \nabla^2 U = -\frac{\rho_e}{\varepsilon_f} = -\frac{e\sum_i z_i n_i}{\varepsilon_f} \quad (5)$$

In the above equation, $\vec{E}$ is the electric field, U is the electrical potential, ρ_e is the net charge density, ε_f is permittivity of the fluid, n_i is the concentration of the ith ionic species, and z_i is the valency.

(2) Steady-state Navier−Stokes equation for liquid motion:

$$\rho\vec{v}\cdot\nabla\vec{v} = -\nabla p + \mu\nabla^2\vec{v} + e\sum_i z_i n_i \vec{E} \quad (6)$$

where $\vec{v}$ is the velocity of the liquid, p is the hydrostatic pressure, and μ is the fluid viscosity.

(3) Steady-state Nernst−Plank equation for ion motion:

$$\nabla\cdot\vec{N}_i = \nabla\cdot(n_i\vec{v} - D_i\nabla n_i - \mu_i n_i \nabla U) = 0 \quad (7)$$

$\vec{N}_i$ is the ionic flux density of the ith ionic species, D_i is the diffusivity, and μ_i is the mobility.

Parameters used in the calculation: Electric mobility of double-stranded λ-DNA, $\mu_{DNA} = 4.1 \times 10^{-8}$ m^2/(V s);[39] mobility of K^+ and Cl^-, $\mu_K = 7.616 \times 10^{-8}$ m^2/sV and $\mu_{Cl} = 7.909 \times 10^{-8}$ m^2/sV; solution permittivity, $\varepsilon_f = 7.08 \times 10^{-10}$ F/m; fluid viscosity, $\mu = 8.91 \times 10^{-4}$ Pa·s.

Acknowledgment. This research is supported partially by the Japan Society for the Promotion of Science (JSPS) through its "Funding Program for World-Leading Innovative R&D on Science and Technology".

Supporting Information Available: Dependence of voltage residue ratio on nanopore radius, estimation with experiments, and evaluation of λ-DNA diffusion velocity. This material is available free of charge *via* the Internet at http://pubs.acs.org.

REFERENCES AND NOTES

1. Craighead, H. *Nature* **2006**, *442*, 387–393.
2. Dekker, C. *Nat. Nanotechnol.* **2007**, *2*, 209–215.
3. Zwolak, M.; Di Ventra, M. *Rev. Mod. Phys.* **2008**, *80*, 141–165.
4. Branton, D.; Deamer, D. W.; Marziali, A.; Bayley, H.; Benner, S. A.; Butler, T.; Di Ventra, M.; Garaj, S.; Hibbs, A.; Huang, X.; Jovanovich, S. B.; Krstic, P. S.; Lindsay, S.; Ling, X. S.; Mastrangelo, C. H.; *et al*. *Nat. Biotechnol.* **2008**, *26*, 1146–1153.
5. Clarke, J.; Wu, H.-C.; Jayasinghe, L.; Patel, A.; Reid, S.; Bayley, H. *Nat. Nanotechnol.* **2009**, *4*, 265–270.
6. Kasianowicz, J. J.; Brandin, E.; Branton, D.; Deamer, D. W. *Proc. Natl. Acad. Sci. U. S. A.* **1996**, *93*, 13770–13773.
7. Akeson, M.; Branton, D.; Kasianowicz, J. J.; Brandin, E.; Deamer, D. W. *Biophys. J.* **1999**, *77*, 3227–3233.
8. Meller, A.; Nivon, L.; Brandin, E.; Golovchenko, J.; Branton, D. *Proc. Natl. Acad. Sci. U. S. A.* **2000**, *97*, 1079–1084.
9. Zwolak, M.; Di Ventra, M. *Nano Lett.* **2005**, *5*, 421–424.
10. Lagerqvist, J.; Zwolak, M.; Di Ventra, M. *Nano Lett.* **2006**, *6*, 779–782.
11. Tsutsui, M.; Taniguchi, M.; Yokota, K.; Kawai, T. *Nat. Nanotechnol.* **2010**, *5*, 286–290.
12. Li, J.; Gershow, M.; Stein, D.; Brandin, E.; Golovchenko, J. A. *Nat. Mater.* **2003**, *2*, 611–615.
13. Chen, P.; Mitsui, T.; Farmer, D. B.; Golovchenko, J.; Gordon, R. G.; Branton, D. *Nano Lett.* **2004**, *4*, 1333–1337.
14. Chen, P.; Gu, J.; Brandin, E.; Kim, Y.-R.; Wang, Q.; Branton, D. *Nano Lett.* **2004**, *4*, 2293–2298.
15. Venkatesan, B. M.; Shah, A. B.; Zuo, J.-M.; Bashir, R. *Adv. Funct. Mater.* **2010**, *20*, 1266–1275.
16. Nakane, J.; Akeson, M.; Marziali, A. *Electrophoresis* **2002**, *23*, 2592–2601.
17. Grosberg, A. Y.; Rabin, Y. *J. Chem. Phys.* **2010**, *133*, 165102.
18. Wanunu, M.; Morrison, W.; Rabin, Y.; Grosberg, A. Y.; Meller, A. *Nat. Nanotechnol.* **2010**, *5*, 160–165.
19. Wong, C. T. A.; Muthukumar, M. *J. Chem. Phys.* **2007**, *126*, 164903.
20. Muthukumar, M. *J. Chem. Phys.* **2010**, *132*, 195101.
21. Smeets, R. M. M.; Keyser, U. F.; Krapf, D.; Wu, M.-Y.; Dekker, N. H.; Dekker, C. *Nano Lett.* **2006**, *6*, 89–95.
22. Keyser, U. F.; Koeleman, B. N.; van Dorp, S.; Krapf, D.; Smeets, R. M. M.; Lemay, S. G.; Dekker, N. H.; Dekker, C. *Nat. Phys.* **2006**, *2*, 473–477.
23. Skinner, G. M.; van den Hout, M.; Broekmans, O.; Dekker, C.; Dekker, N. H. *Nano Lett.* **2009**, *9*, 2953–2960.
24. van Dorp, S.; Keyser, U. F.; Dekker, N. H.; Dekker, C.; Lemay, S. G. *Nat. Phys.* **2009**, *5*, 347–351.
25. Behrens, S. H.; Grier, D. G. *J. Chem. Phys.* **2001**, *115*, 6716–6721.
26. Alami-Younssi, S.; Larbot, A.; Persin, M.; Sarrazin, J.; Cot, L. *J. Membr. Sci.* **1995**, *102*, 123–129.
27. Ghosal, S. *Phys. Rev. Lett.* **2007**, *98*, 238104.
28. Postma, H. W. C. *Nano Lett.* **2010**, *10*, 420–425.
29. Garaj, S.; Hubbard, W.; Reina, A.; Kong, J.; Branton, D.; Golovchenko, J. A. *Nature* **2010**, *467*, 190–193.
30. Merchant, C. A.; Healy, K.; Wanunu, M.; Ray, V.; Peterman, N.; Bartel, J.; Fischbein, M. D.; Venta, K.; Luo, Z.; Johnson, A. T. C.; Drndic, M. *Nano Lett.* **2010**, *10*, 2915–2921.
31. Schneider, G. F.; Kowalczyk, S. W.; Calado, V. E.; Pandraud, G.; Zandbergen, H. W.; Vandersypen, L. M. K.; Dekker, C. *Nano Lett.* **2010**, *10*, 3163–3167.
32. Min, S. K.; Kim, W. Y.; Cho, Y.; Kim, K. S. *Nat. Nanotechnol.* **2011**, *6*, 162–165.
33. Prasongkit, J.; Grigoriev, A.; Pathak, B.; Ahuja, R.; Scheicher, R. H. *Nano Lett.* **2011**, *11*, 1941–1945.
34. Kumara, R.; Muthukumar, M. *J. Chem. Phys.* **2009**, *131*, 194903.
35. de Gennes, P.-G. *J. Chem. Phys.* **1974**, *60*, 5030.
36. Nam, S.-W.; Rooks, M. J.; Kim, K.-B.; Rossnagel, S. M. *Nano Lett.* **2009**, *9*, 2044–2048.
37. Nam, S.-W.; Lee, M.-H.; Lee, S.-H.; Lee, D.-J.; Rossnagel, S. M.; Kim, K.-B. *Nano Lett.* **2010**, *10*, 3324–3329.
38. He, Y.; Tsutsui, M.; Fan, C.; Taniguchi, M.; Kawai, T. *ACS Nano* **2011**, *5*, 5509–5518.
39. Nkodo, A. E.; Garnier, J. M.; Tinland, B.; Ren, H.; Desruisseaux, C.; McCormick, L. C.; Drouin, G.; Slater, G. W. *Electrophoresis* **2001**, *22*, 2424–2432.